Ionic Liquid-Assisted Growth of Single-Crystalline Dendritic Gold Nanostructures with a Three-Fold Symmetry

Yao Qin, Yin Song, Nijuan Sun, Nana Zhao, Meixian Li, and Limin Qi*

Beijing National Laboratory for Molecular Sciences, State Key Laboratory for Structural Chemistry of Unstable and Stable Species, College of Chemistry, Peking University, Beijing 100871, People's Republic of China

Received January 24, 2008. Revised Manuscript Received April 23, 2008

Hierarchical, three-fold symmetrical, single-crystalline gold dendrites were synthesized by the reaction between a zinc plate and a solution of $HAuCl_4$ in the ionic liquid [BMIM][PF_6]. The unique dendritic gold nanostructures show a three-order hierarchy (i.e., a three-fold symmetrical <111>-oriented trunk, three groups of trident-like <111>-oriented branches grown on the trunk, and many <111>-oriented nanorod leaves grown on the branches symmetrically), indicating an interesting fractal growth. According to the investigation on the growth process of the gold dendrites, it was proposed that gold nuclei nanocrystals first formed on the zinc substrate through a direct surface reaction and that the subsequent crystal growth preferentially took place on the preformed gold crystals through a primary cell reaction, leading to the formation of the final hyperbranched dendrites under nonequilibrium conditions. In contrast, AuZn alloy dendrites consisting of aggregated primary nanoparticles were produced when the ionic liquid solution was replaced by an aqueous solution. It was proposed that the significantly lowered ion diffusivity and reaction rate in the ionic liquid medium could largely contribute to the formation of the pure single-crystalline gold dendrites. Moreover, electrocatalytic measurements performed in alkaline solution suggested that the obtained dendritic gold nanostructures exhibited good electrocatalytic activity toward the oxidation of methanol, which might be related to the special three-order hierarchical architectures.

Introduction

Ionic liquids (ILs) are organic salts with melting points near room temperature, which have received a great deal of attention as green and designer solvents owing to their unique properties such as negligible vapor pressure, nonflammability, high chemical and thermal stability, high polarity, high ionic conductivity, wide electrochemical window, and tunable physicochemical properties including dissolving ability and solvent miscibility.[1] While ILs widely have been used in organic and polymer synthesis, electrochemistry, catalysis, and separation, the synthesis of inorganic materials in ILs is a rather new development and has attracted increasing interest in recent years.[2] A variety of transition-metal nanoparticles was synthesized in ILs to form stable dispersions,[3] and the catalytic applications of metal nanoparticles dispersed in ILs were demonstrated.[4] By using ILs as reaction media, Au nanosheets,[5] CoPt alloy nanorods,[6] metal oxide[7] and chalcogenide[8] nanostructures, and cyano-bridged magnetic nanoparticles[9] successfully were prepared. Because of their high polarizability, ILs are used as microwave absorbents for the rapid synthesis of Te nanorods,[10a] manganese oxide nanoneedles,[10b] metal fluoride nanoparticles,[10c] high-quality TiO_2 nanocrystals,[10d] and luminescent $LaPO_4$:Ce,Te nanocrystals.[10e] Ionothermal synthesis of hierarchical ZnO nanostructures[11] and novel molecular sieve materials[12] in ILs

* Corresponding author. E-mail: liminqi@pku.edu.cn.

(1) (a) Weingrtner, H. *Angew. Chem., Int. Ed.* **2008**, *47*, 654. (b) Pârvulescu, V. I.; Hardacre, C. *Chem. Rev.* **2007**, *107*, 2615. (c) van Rantwijk, F.; Sheldon, R. A. *Chem. Rev.* **2007**, *107*, 2757. (d) Lee, S. *Chem. Commun. (Cambridge, U.K.)* **2006**, 1049.

(2) (a) Antonietti, M.; Kuang, D.; Smarsly, B.; Zhou, Y. *Angew. Chem., Int. Ed.* **2004**, *43*, 4988. (b) Tauber, A.; Li, Z. *Dalton Trans.* **2007**, 723. (c) Morris, R. E. *Angew. Chem., Int. Ed.* **2008**, *47*, 442. (d) Abbott, A. P.; McKenzie, K. J. *Phys. Chem. Chem. Phys.* **2006**, *8*, 4265.

(3) (a) Dupont, J.; Fonseca, G. S.; Umpierre, A. P.; Fichtner, P. F. P.; Teixeira, S. R. *J. Am. Chem. Soc.* **2002**, *124*, 4228. (b) Gelesky, M. A.; Umpierre, A. P.; Machado, G.; Correia, R. R. B.; Magno, W. C.; Morais, J.; Ebeling, G.; Dupont, J. *J. Am. Chem. Soc.* **2005**, *127*, 4588. (c) Kim, K. S.; Demberelnyamba, D.; Lee, H. *Langmuir* **2004**, *20*, 556. (d) Mu, X.-d.; Meng, J.-q.; Li, Z.-C.; Kou, Y. *J. Am. Chem. Soc.* **2005**, *127*, 9694. (e) Zhao, D.; Fei, Z.; Ang, W. H.; Dyson, P. L. *Small* **2006**, *2*, 879.

(4) Migowski, P.; Dupont, J. *Chem.—Eur. J.* **2007**, *13*, 32.

(5) (a) Li, Z.; Liu, Z.; Zhang, J.; Han, B.; Du, J.; Gao, Y.; Jiang, T. *J. Phys. Chem. B* **2005**, *109*, 14445. (b) Zhu, J.; Shen, Y.; Xie, A.; Qiu, L.; Zhang, Q.; Zhang, S. *J. Phys. Chem. C* **2007**, *111*, 7629.

(6) Wang, Y.; Yang, H. *J. Am. Chem. Soc.* **2005**, *127*, 5316.

(7) (a) Zhou, Y.; Antonietti, M. *J. Am. Chem. Soc.* **2003**, *125*, 14960. (b) Kaper, H.; Endres, F.; Djerdj, I.; Antonietti, M.; Smarsly, B. M.; Maier, J.; Hu, Y.-S. *Small* **2007**, *3*, 1753. (c) Wang, Y.; Maksimuk, S.; Shen, R.; Yang, H. *Green Chem.* **2007**, *9*, 1051.

(8) (a) Jiang, J.; Yu, S.-H.; Yao, W.-T.; Ge, H.; Zhang, G.-Z. *Chem. Mater.* **2005**, *17*, 6094. (b) Biswas, K.; Rao, C. N. R. *Chem.—Eur. J.* **2007**, *13*, 6123.

(9) Clavel, G.; Larionova, J.; Guari, Y.; Guérin, C. *Chem.—Eur. J.* **2006**, *12*, 3798.

(10) (a) Zhu, Y.-J.; Wang, W.-W.; Qi, R.-J.; Hu, X.-L. *Angew. Chem., Int. Ed.* **2004**, *43*, 1410. (b) Yang, L.-X.; Zhu, Y.-J.; Wang, W.-W.; Tong, H.; Ruan, M.-L. *J. Phys. Chem. B* **2006**, *110*, 6609. (c) Jacob, D. S.; Bitton, L.; Grinblat, J.; Felner, I.; Koltypin, Y.; Gedanken, A. *Chem. Mater.* **2006**, *18*, 3162. (d) Ding, K.; Miao, Z.; Liu, Z.; Zhang, Z.; Han, B.; An, G.; Miao, S.; Xie, Y. *J. Am. Chem. Soc.* **2007**, *129*, 6362. (e) Bühler, G.; Feldmann, C. *Angew. Chem., Int. Ed.* **2006**, *45*, 4864.

(11) Zhu, H.; Huang, J.-F.; Pan, Z.; Dai, S. *Chem. Mater.* **2006**, *18*, 4473.

(12) (a) Parnham, E. R.; Morris, R. E. *Chem. Mater.* **2006**, *18*, 4882. (b) Cai, R.; Sun, M.; Chen, Z.; Munoz, R.; O'Neil, C.; Beving, D. E.; Yan, Y. *Angew. Chem., Int. Ed.* **2008**, *47*, 525.

10.1021/cm8002386 CCC: $40.75
Published on Web 05/21/2008

at high temperature also were realized owing to their low vapor pressure. Notably, organized structures formed by ILs were used as templates for the synthesis of various mesoporous materials[13] and hollow TiO_2 microspheres;[14] moreover, CuCl nanoplatelets[15] and metal nanoparticles[16] were obtained from ionic liquid-crystal precursors. Nevertheless, the potential of ILs in the controlled synthesis of inorganic nanostructures with a complex form or hierarchical architectures remains to be fully explored.

Gold nanostructures have stimulated great research because of their fascinating optical, electronic, and chemical properties and promising applications in nanoelectronics, biomedicine, sensing, and catalysis.[17] Since the intrinsic properties and relevant applications of gold nanostructures are determined by their size and shape, great efforts have been devoted to the morphology-controlled synthesis of gold nanostructures in recent years.[18] In particular, a variety of wet chemical methods was developed to fabricate gold nanoparticles with various shapes such as rods,[19] wires,[20] belts,[21] sheets,[5,22] prisms,[23] cubes,[24] polyhedra,[25] and branched particles.[26] However, it remains a challenge to synthesize gold nanostructures with hierarchical architectures, which is a crucial step toward integrating nanoscale gold building blocks into complex functional devices. In this regard, single-crystalline, comb-like gold nanostructures successfully were obtained in aqueous mixed surfactant solutions.[21b] It is worth noting that dendritic nanostructures with hyperbranched architectures have attracted much attention due to their importance in understanding the fascinating fractal growth phenomena and their potential applications in functional devices, plasmonics, biosensing, and catalysis; recent examples include the hierarchical nanodendrites of metals,[27] oxides,[28] and sulfides[29] formed in solution systems. However, there are rare reports on the dendritic gold nanostructures of the hyperbranched type. A notable example is the formation of nanoparticle-aggregated dendritic gold nanostructures through a fast electroless metal deposition route in aqueous solutions.[30] It would be highly desirable to realize the controlled synthesis of single-crystalline dendritic gold nanostructures with a well-defined crystal orientation. Furthermore, it is worthwhile to explore the fractal growth behavior of gold in ILs.

Herein, we report the large-scale growth of hierarchical, three-fold symmetrical, single-crystalline gold dendrites on zinc substrate in the ionic liquid 1-butyl-3-methylimidazolium hexafluorophosphate ([BMIM][PF_6]). Structural characterizations suggest that the unique dendritic gold nanostructures have a three-order hierarchy (i.e., a three-fold symmetrical <111>-oriented trunk, trident-like <111>-oriented branches, and <111>-oriented nanorod leaves). Moreover, it has been shown that the obtained dendritic gold nanostructures exhibit a good electrocatalytic activity toward the oxidation of methanol.

Experimental Procedures

Materials. Tetrachloroauric acid tetrahydrate ($HAuCl_4 \cdot 4H_2O$, AR) was obtained from Beijing Chemical Reagent Co. Ltd. [BMIM][PF_6] was purchased from Henan Lihua Pharmaceutical Co. of China (99%). These chemicals were used without further purification. Zinc foil (1 mm in thickness, 99.99%) was purchased from Alfa Aesar and treated by sonication in acetone and water successively to remove surface contamination and dried in air.

Synthesis. $HAuCl_4 \cdot 4H_2O$ was first dissolved in [BMIM][PF_6] to obtain a clear solution of a certain concentration in a plastic

(13) (a) Zhou, Y.; Schattka, J. H.; Antonietti, M. *Nano Lett.* **2004**, *4*, 477. (b) Trewyn, B. G.; Whitman, C. M.; Lin, V. S.-Y. *Nano Lett.* **2004**, *4*, 2139. (c) Brezensinski, T.; Erpen, C.; Iimura, K.; Smarsly, B. *Chem. Mater.* **2005**, *17*, 1683. (d) Wang, T.; Kaper, H.; Antonietti, M.; Smarsly, B. *Langmuir* **2007**, *23*, 1489. (e) Park, H.; Yang, S. H.; Jun, Y.-S.; Hong, W. H.; Kang, J. K. *Chem. Mater.* **2007**, *19*, 535.

(14) Nakashima, T.; Kimizuka, N. *J. Am. Chem. Soc.* **2003**, *125*, 6386.

(15) Taubert, A. *Angew.Chem., Int. Ed.* **2004**, *43*, 5380.

(16) Dobbs, W.; Suisse, J.-M.; Douce, L.; Welter, R. *Angew.Chem., Int. Ed.* **2006**, *45*, 4179.

(17) (a) Daniel, M.-C.; Astruc, D. *Chem. Rev.* **2004**, *104*, 293. (b) Hu, M.; Chen, J.; Li, Z.-Y.; Au, L.; Hartland, G. V.; Li, X.; Marguez, M.; Xia, Y. *Chem. Soc. Rev.* **2006**, *35*, 1084.

(18) (a) Wiley, B.; Sun, Y.; Chen, J.; Cang, H.; Li, Z.-Y.; Li, X.; Xia, Y. *MRS Bull.* **2005**, *30*, 356. (b) Chen, J.; Wiley, B. J.; Xia, Y. *Langmuir* **2007**, *23*, 4120. (c) Murphy, C. J.; Sau, T. K.; Gole, A. M.; Orendorff, C. J.; Gao, J.; Gou, L.; Hunyadi, S. E.; Li, T. *J. Phys. Chem. B* **2005**, *109*, 13857. (d) Murphy, C. J.; Gole, A. M.; Hungyadi, S. E.; Orendorff, C. J. *Inorg. Chem.* **2006**, *45*, 7544.

(19) (a) Jana, N.; Gearheart, L.; Murphy, C. *J. Phys. Chem. B* **2001**, *105*, 4065. (b) Kim, F.; Song, J. H.; Yang, P. *J. Am. Chem. Soc.* **2002**, *124*, 14316. (c) Kou, X.; Zhang, S.; Tsung, C.-K.; Yang, Z.; Yeung, M. H.; Stucky, G. D.; Sun, L.; Wang, J.; Yan, C. *Chem.—Eur. J.* **2007**, *13*, 2929. (d) Iqbal, M.; Chung, Y. I.; Tae, G. Y. *J. Mater. Chem.* **2007**, *17*, 335.

(20) (a) Kim, J.-U.; Cha, S.-H.; Shin, K.; Jho, J. Y.; Lee, J.-C. *Adv. Mater.* **2004**, *16*, 459. (b) Vasilev, K.; Zhu, T.; Wilms, M.; Gillies, G.; Lieberwirth, I.; Mittler, S.; Knoll, W.; Kreiter, M. *Langmuir* **2005**, *21*, 12399. (c) Halder, A.; Ravishankar, N. *Adv. Mater.* **2007**, *19*, 1854.

(21) (a) Zhang, J.; Du, J.; Han, B.; Liu, Z.; Jiang, T.; Zhang, Z. *Angew. Chem., Int. Ed.* **2006**, *45*, 1116. (b) Zhao, N.; Wei, Y.; Sun, N.; Chen, Q.; Bai, J.; Zhou, L.; Qin, Y.; Li, M.; Qi, L. *Langmuir* **2008**, *24*, 991.

(22) (a) Sun, X.; Dong, S.; Wang, E. *Angew. Chem., Int. Ed.* **2004**, *43*, 6360. (b) Shao, Y.; Jin, Y.; Dong, S. *Chem. Commun. (Cambridge, U.K.)* **2004**, 1104.

(23) (a) Millstone, J. E.; Park, S.; Shuford, K. L.; Qin, L.; Schatz, G. C.; Mirkin, C. A. *J. Am. Chem. Soc.* **2005**, *127*, 5312. (b) Ha, T. W.; Koo, H. J.; Chung, B. H. *J. Phys. Chem. C* **2007**, *111*, 1123. (c) Jena, B. K.; Raj, C. R. *J. Phys. Chem. C* **2007**, *111*, 15146.

(24) Jin, R.; Egusa, S.; Scherer, N. F. *J. Am. Chem. Soc.* **2004**, *126*, 9900.

(25) (a) Kim, F.; Connor, S.; Song, H.; Kuykendall, T.; Yang, P. *Angew. Chem., Int. Ed.* **2004**, *43*, 3673. (b) Seo, D.; Park, J. C.; Song, H. *J. Am. Chem. Soc.* **2006**, *128*, 14863. (c) Li, C.; Shuford, K. L.; Park, Q. H.; Cai, W.; Li, Y.; Lee, E. J.; Cho, S. O. *Angew. Chem., Int. Ed.* **2007**, *46*, 3264.

(26) (a) Chen, S.; Wang, Z. L.; Ballato, J.; Foulger, S. H.; Carroll, D. L. *J. Am. Chem. Soc.* **2003**, *125*, 16186. (b) Hao, E.; Bailey, R. C.; Schatz, G. C.; Hupp, J. T.; Li, S. *Nano Lett.* **2004**, *4*, 327. (c) Chen, H. M.; Hsin, C. F.; Liu, R.-S.; Lee, J.-F.; Jang, L.-Y. *J. Phys. Chem. C* **2007**, *111*, 5909. (d) Krichevski, O.; Markovich, G. *Langmuir* **2007**, *23*, 1496. (e) Jena, B. K.; Raj, C. R. *Langmuir* **2007**, *23*, 4064. (f) Li, Z.; Ravaine, V.; Ravaine, S. R.; Garrigue, P.; Kuhn, A. *Adv. Funct. Mater.* **2007**, *17*, 618. (g) Yuan, H.; Ma, W.; Chen, C.; Zhao, J.; Liu, J.; Zhu, H.; Gao, X. *Chem. Mater.* **2007**, *19*, 1592. (h) Xie, J.; Lee, J. Y.; Wang, D. I. C. *Chem. Mater.* **2007**, *19*, 2823. (i) Lu, G.; Li, C.; Shi, G. *Chem. Mater.* **2007**, *19*, 3433.

(27) (a) Wen, X.; Xie, Y.-T.; Mak, M. W. C.; Cheung, K. Y.; Li, X.-Y.; Renneberg, R.; Yang, S. *Langmuir* **2006**, *22*, 4836. (b) Qiu, R.; Zhang, X. L.; Qiao, R.; Li, Y.; Kim, Y. I.; Kang, Y. S. *Chem. Mater.* **2007**, *19*, 4174. (c) Fang, J.; You, H.; Kong, P.; Yi, Y.; Song, X.; Ding, B. *Cryst. Growth Des.* **2007**, *7*, 864.

(28) (a) Cao, M.; Liu, T.; Gao, S.; Sun, G.; Wu, X.; Hu, C.; Wang, Z. L. *Angew. Chem., Int. Ed.* **2005**, *44*, 4197. (b) Hu, X.; Yu, J. C.; Gong, J. *J. Phys. Chem. C* **2007**, *111*, 11180. (c) Li, G.-R.; Lu, X.-H.; Qu, D.-L.; Yao, C.-Z.; Zheng, F.-L.; Bu, Q.; Dawa, C.-R.; Tong, Y.-X. *J. Phys. Chem. C* **2007**, *111*, 6678.

(29) (a) Kuang, D.; Xu, A.; Fang, Y.; Liu, H.; Frommen, C.; Fenske, D. *Adv. Mater.* **2003**, *15*, 1747. (b) Cao, H.; Gong, Q.; Qian, X.; Wang, H.; Zai, J.; Zhu, Z. *Cryst. Growth Des.* **2007**, *7*, 425. (c) Wang, Q.; Xu, G.; Han, G. *Cryst. Growth Des.* **2006**, *6*, 1776.

(30) Fang, J.; Ma, X.; Cai, H.; Song, X.; Ding, B. *Nanotechnology* **2006**, *17*, 5841.

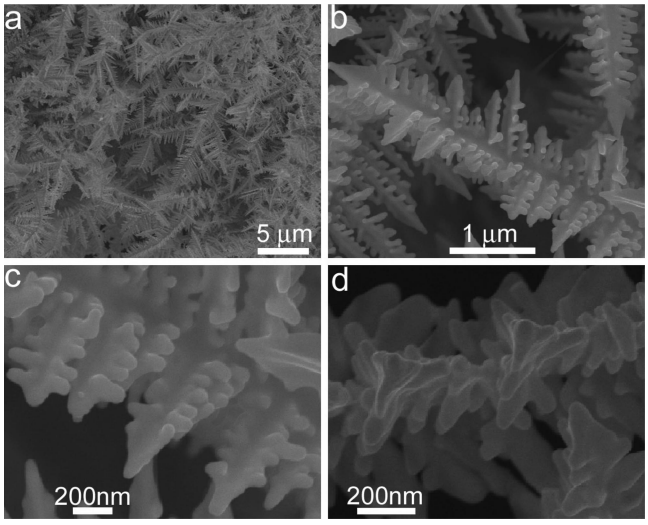

Figure 1. SEM images of gold dendrites grown in [BMIM][PF_6]. [$HAuCl_4$] is 15 mM.

tube. The synthesis of dendritic gold nanostructures was achieved simply by immersing a zinc plate into the [BMIM][PF_6] solution. In a typical synthesis, 1 mL of a 15 mM solution of $HAuCl_4$ in [BMIM][PF_6] was added into a 10 mL plastic tube. A piece of zinc plate (0.5 cm × 0.5 cm) was immersed in the solution, which was then put into an oven at 60 °C and held for 4.5 h. After the reaction, the product was washed with acetone thoroughly and collected for characterization. All the syntheses was conducted under atmosphere without using a drying box to control the water/oxygen level. In the experiments, the $HAuCl_4$ concentration was systematically varied to obtain gold products with modified morphologies.

Characterization. The products obtained were characterized by scanning electron microscopy (SEM, Hitachi S4800, 15 kV), transmission electron microscopy (TEM, JEOL JEM 200CX, 160 kV), and high-resolution TEM (HRTEM, FEI TECNAI F30, 300 kV) together with associated energy-dispersive X-ray spectroscopy (EDS) and powder X-ray diffraction (XRD, Rigaku Dmax-2000, Cu Kα).

Electrochemical Measurements. A CHI 660A electrochemical workstation (Shanghai CH Instruments) with a conventional three-electrode cell was used to perform electrochemical measurements. The working electrode was a glassy carbon electrode with a diameter of 4 mm. A KCl saturated calomel electrode (SCE) was used as the reference electrode and a platinum electrode as the auxiliary electrode. All the electrochemical experiments were conducted at ambient temperature (20 ± 2 °C) under N_2 protection. For the preparation of gold dendrite-modified GC electrodes, the prepared dendritic gold nanostructures were dispersed in deionized water to obtain a uniform suspension of ~2 mg mL^{-1} by sonication. Glassy carbon (GC) electrodes were first polished with 0.3 and 0.05 μm alumina slurries successively and then washed ultrasonically in distilled water and ethanol for 5 min. The GC electrodes were coated by casting 5 μL of the gold nanodendrite suspension and drying naturally in the air. Finally, 4 μL of 0.05 wt % Nafion solution in alcohol was cast on the surface of the sample and dried naturally in the air.

Results and Discussion

Characterization of Dendritic Au Nanostructures. Figure 1 presents typical SEM images of the gold product obtained in a 15 mM solution of $HAuCl_4$ in [BMIM][PF_6] after aging at 60 °C for 4.5 h. As shown in Figure 1a, the product consists almost entirely of hyperbranched dendrites up to more than 10 μm in length. An enlarged image showing a single dendrite is shown in Figure 1b, which suggests that the hierarchical dendrite consists of a pronounced, three-fold symmetrical trunk with three groups of branches grown on the trunk in parallel. Two SEM images with even higher magnifications but different observation directions are presented in Figure 1c,d, which show that each branch has a three-fold symmetrical structure with three groups of parallel rod-like leaves (~50 nm in diameter) grown on the branch symmetrically. These observations suggest that the hierarchical gold dendrites have a three-order structure (i.e., three-fold symmetrical trunk, three-fold symmetrical branches, and parallel leaves made of nanorods). The XRD pattern of the hierarchical dendrites is shown in Figure 2a, which exhibits sharp reflections characteristic of the cubic Au (JCPDS 04-0784), indicating that the dendrites are pure, well-crystallized gold crystals. The EDS spectrum shown in Figure 2b shows only the Au signals except the Cu and C signals arising from the carbon-covered copper grid supporting the gold dendrites, confirming the formation of pure gold crystals.

TEM and HRTEM observations were carried out to determine the crystal orientation of the obtained dendritic gold nanostructures (Figure 3). Figure 3a shows a typical image of the thin tip of the main trunk of an individual gold dendrite lying on the copper grid. The dendrite consisting of three groups of parallel branches stands on the copper grid with two groups of parallel branches touching the grid and one group of parallel branches extending upward, which is consistent with the presence of a dark line along the trunk axis in the TEM image. The selected area electron diffraction (ED) pattern of the trunk tip including some branches shows clear spots indexed to the [$11\bar{2}$] zone axis of cubic gold, indicating that the Au dendrite is a single crystal with the trunk grown along the [111] direction. Because of the 3-D structure of the dendrite, the growth direction of each branch cannot be determined directly by the ED pattern. However, considering that both the trunk and the branches have a three-fold symmetrical structure and that the angle between the trunk and the branches in the TEM image (~68.6°) is identical to the theoretical angle between two equivalent <111> directions of cubic gold in the ($11\bar{2}$) projection plane, the growth direction of each branch may be induced to be the <111> direction (i.e., all branches are <111>-oriented single crystals with a three-fold symmetry). This conclusion is confirmed by the TEM and ED characterization of an individual branch shown in Figure 3b, which suggests that each trident-like branch is actually a single crystal grown along the [111] direction, like a miniature of the trunk. Similarly, it can be inferred that each nanorod leaf is also a single crystal elongated along the <111> direction. The single-crystalline nature of the dendrite is further demonstrated by careful HRTEM investigation of the branch. As shown in Figure 3c,d, the leaf tip denoted as A and the branch edge denoted as B in Figure 3b exhibit lattice fringes with the same orientation and the same spacing (i.e., 0.24 nm), which is in good agreement with the *d* values of the (111) lattice spacing of cubic gold crystals (0.235 nm). Therefore, it may

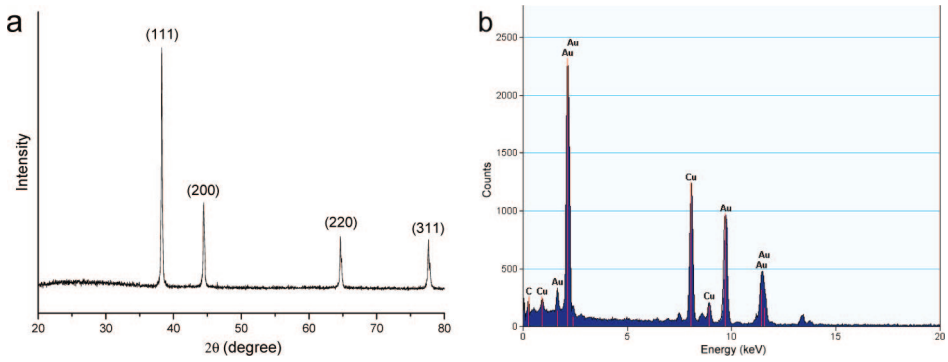

Figure 2. XRD pattern (a) and EDS spectrum (b) of gold dendrites grown in [BMIM][PF_6].

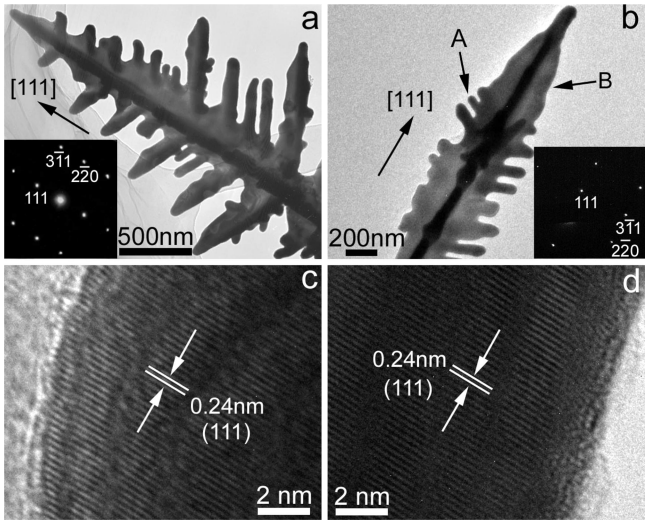

Figure 3. TEM images of the trunk tip of a gold dendrite (a) and a branch with rod-like leaves (b). Panels c and d show the HRTEM images of the leaf tip denoted as A and the branch edge denoted as B in panel b, respectively. Insets show the ED patterns corresponding to the whole area of the related image.

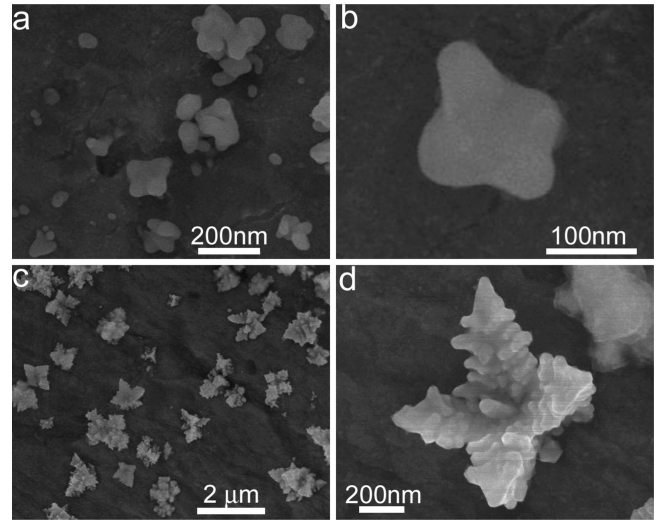

Figure 4. SEM images of gold products obtained at earlier stages of formation of gold dendrites in [BMIM][PF_6]. Reaction time: (a and b) 10 min and (c and d) 1 h.

Scheme 1. Schematic Illustration of Growth Process of Gold Dendrites on Zinc Substrate

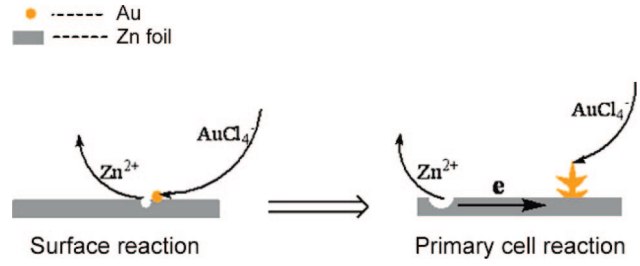

be concluded that the entire dendrite with a three-fold symmetry is a single crystal showing a three-order hierarchical structure (i.e., a <111>-oriented trunk, three groups of <111>-oriented branches grown on the trunk, and many <111>-oriented nanorod leaves grown on the branches), indicating an interesting fractal growth. To the best of our knowledge, it is for the first time that such well-defined, three-fold symmetrical, single-crystalline dendrites with <111>-oriented trunks, branches, and leaves have been synthesized for gold.

Growth Process of Dendritic Au Nanostructures. Figure 4 shows the gold products grown on the zinc substrate at the earlier growth stages of the gold dendrites. After 10 min of reaction, gold nanocrystals of ~50−200 nm formed on the zinc substrate, and some of them look like buds with several rudimental petals (Figure 4a,b). When the reaction time was prolonged to 1 h, many micrometer-sized flower-like crystals with dentation-structured petals appeared on the substrate (Figure 4c), indicating further growth from the original bud-like crystals. An enlarged SEM image of an individual flower-like crystal is shown in Figure 4d, which suggests that each petal shows a three-fold symmetrical structure with three groups of side branches grown on the stem. Each petal would finally evolve into a complex three-fold symmetrical dendrite with a three-order hierarchy as shown in Figure 1 after 4.5 h of reaction.

According to the previous observation, a growth process is tentatively proposed for the formation of the dendritic gold nanostructures (Scheme 1). When the zinc plate was immersed in a solution of $HAuCl_4$ in [BMIM][PF_6], the following reaction between Zn and $HAuCl_4$ occurred on the zinc surface: $2[AuCl_4]^- + 3Zn \rightarrow 2Au + 3Zn^{2+} + 8Cl^-$, resulting in the formation of primary gold nanocrystals on the zinc substrate as nuclei, which was accompanied by the release of Zn^{2+} ions into the IL solution. The subsequent growth of gold crystals would preferentially take place on the preformed gold nuclei through a primary cell reaction rather than on bare zinc surfaces through a surface reaction

possibly due to the relatively high activation energy for the surface reaction. Namely, a primary electric cell, which consisted of the Zn anode, Au cathode, and IL containg the Zn^{2+} and $[AuCl_4]^-$ ions as the electrolyte, formed spontanously, and the electrode reaction occurred as follows: (anode) $3Zn - 6e \rightarrow 3Zn^{2+}$ and (cathode) $2[AuCl_4]^- + 6e \rightarrow 2Au + 8Cl^-$.

The continuous cathode reaction leads to the gradual electrochemical deposition of gold onto the existing gold buds, which evolved into the final hierarchical, three-fold symmetrical, single-crystalline dendrites under the current nonequilibrium conditions. It was documented that hierarchical branching morphologies are generally formed through a self-organization process under nonequilibrium conditions and that the crystallization pattern is generally affected by the distance between the growth condition and the equilibrium state (i.e., the driving force for crystallization).[31] A delicate balance between the diffusion rate and the reaction rate could be responsible for the formation of highly symmetrical dendrites with a single-crystalline structure. In the present situation, both the diffusion rate of the reactant ions and the electrode reaction rate were affected considerably by the IL [BMIM][PF_6], which could result in a suitable balance between the diffusion rate and the reaction rate, which favored the formation of the unique three-fold symmetrical gold dendrites. An appropriate reversible potential for the metal substrate is essential to the formation of well-defined gold dendrites on a metal substrate. Our preliminary experimental results have shown that the metals with a relatively weaker reducing ability (e.g., Cu and Ni) cannot be used as effective metal substrates for the deposition of Au crystals from $HAuCl_4$ solutions in [BMIM][PF_6] as the reaction would be too slow. In this regard, Zn seems to be unique since it is relatively stable under the atmosphere and shows enough reaction activity toward the reduction of $HAuCl_4$ in the IL [BMIM][PF_6].

Effects of $HAuCl_4$ Concentration. The concentration of $HAuCl_4$ in the IL showed a considerable effect on the formation of dendritic gold structures (Figure 5). When the $HAuCl_4$ concentration was decreased from the standard concentration (15 mM) to 5 mM, the product consisted of irregular dendrites and many unusual four-branched dendrites (Figure 5a). As shown in Figure 5b, these four-branched dendrites have two pairs of branches grown along the trunk axis with each pair of branches perpendicular to the other pair. A high-magnification image (Figure 5c) suggests that each branch shows a fence-like structure. The ED pattern of a single dendrite reveals that the dendrite is a single crystal grown along the $[1\bar{1}0]$ direction with one pair of branches parallel to the [111] direction and the other pair perpendicular to the [111] direction. It is indicated that gold crystals preferentially grow along the <110> direction rather than the <111> direction at a low reactant concentration in ILs. Under a thermodynamic balance, cubic metal crystals grow faster along the <110> direction than the <111> direction.[32] Therefore, it may be reasonably speculated that a lower reactant concentration would lead to a reaction condition

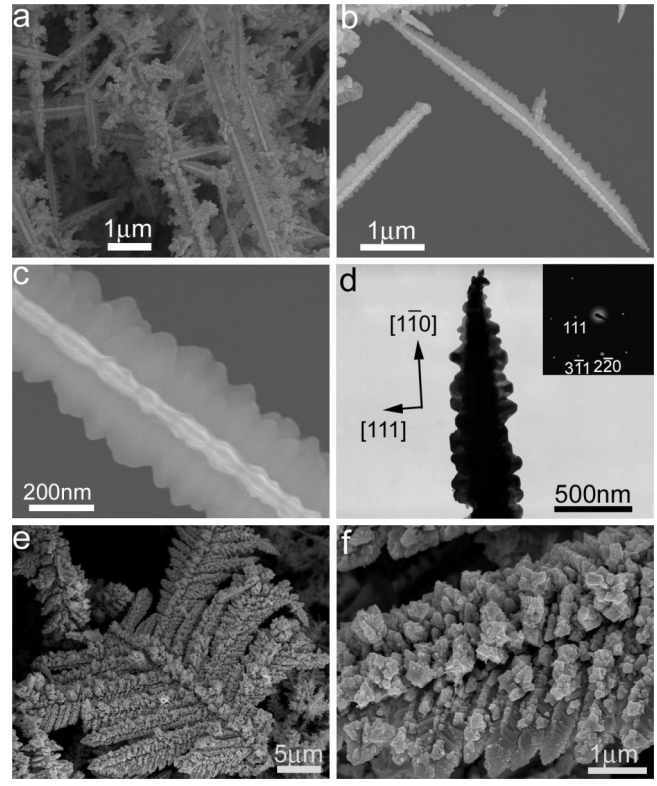

Figure 5. SEM (a−c, e, and f) and TEM (d) images of gold dendrites obtained in [BMIM][PF_6] at different $HAuCl_4$ concentrations: (a−d) 5 mM and (e and f) 35 mM.

closer to the thermodynamic balance, resulting in the formation of the <110>-oriented dendrites due to the relatively faster growth rate along the <110> direction. When the $HAuCl_4$ concentration was increased to 15 mM, the reaction was accelerated, and hence, the reaction condition considerably deviated from the thermodynamic balance, leading to the formation of typical three-fold symmetrical dendrites shown in Figure 1. On increasing the $HAuCl_4$ concentration to 35 mM or higher, the yield of the well-defined, three-fold symmetrical dendrites decreased greatly, and some large, coarse gold dendrites appeared (Figure 5e,f), which could be partly ascribed to the uncontrolled growth of gold crystals due to the high reactant concentration. Meanwhile, the presence of water in the ionic liquid might play a role in the formation of gold dendrites since a small amount of water could have a considerable impact on the physical and chemical properties of the solvent. The water content in the original ionic liquid [BMIM][PF_6] was measured to be 0.15 wt % via a Karl Fisher titration. Since the $HAuCl_4$ solution in [BMIM][PF_6] was prepared by dissolving $HAuCl_4 \cdot 4H_2O$ in the IL, water contents of ~0.23 and 0.33 wt % can be estimated for the 15 and 35 mM $HAuCl_4$ solutions in [BMIM][PF_6], respectively. However, our preliminary experimental results showed that a slight variation of the water content did not show a considerable effect on the formation of gold dendrites. In particular, the reaction carried out in 15 mM $HAuCl_4$ solutions with additional 0.1 wt % water added separately, which corresponded to a total water content of ~0.33 wt %, resulted in the formation of typical three-fold symmetrical dendrites,

(31) Imai, H. *Top. Curr. Chem.* **2007**, *270*, 43.
(32) Wang, Z. L. *J. Phys. Chem. B* **2000**, *104*, 1153.

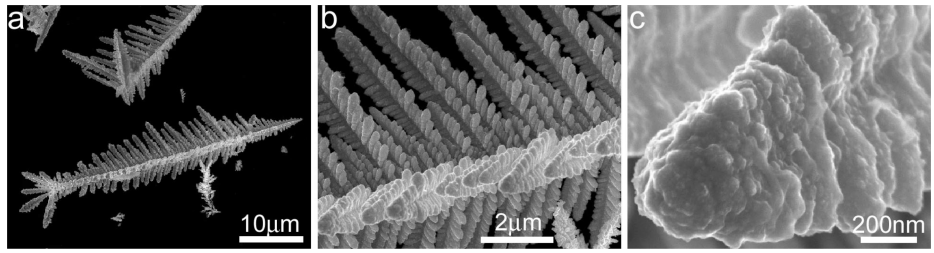

Figure 6. SEM images of AuZn alloy dendrites obtained in aqueous solution.

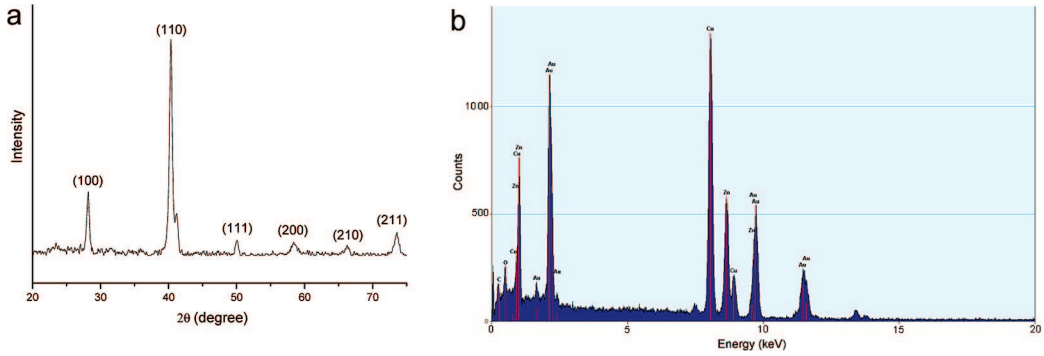

Figure 7. XRD pattern (a) and EDS spectrum (b) of AuZn alloy dendrites obtained in aqueous solution.

similar to those shown in Figure 1. Therefore, the presence of water in the IL may not contribute considerably to the morphological change from the three-fold symmetrical dendrites to the large, coarse dendrites with increasing the $HAuCl_4$ concentration from 15 to 35 mM.

AuZn Alloy Dendrites Grown in Aqueous Solution. For comparison purposes, the reaction between zinc and $HAuCl_4$ also was carried out in aqueous solution by immersing zinc plates in an aqueous $HAuCl_4$ solution instead of the solution of $HAuCl_4$ in [BMIM][PF_6]. Similar to the synthesis procedure conducted in the IL, 1 mL of 15 mM aqueous $HAuCl_4$ solution (pH 1.98) was added to a 10 mL test tube. A piece of zinc plate was then immersed in the solution, which was put into an oven at 60 °C and held for 4.5 h. It was found that the reaction conducted in aqueous solution was much faster than that in the IL solution, resulting in the formation of a mixture of irregular crystals. The reaction was further repeated by immersing the zinc plate in a 15 mM aqueous $HAuCl_4$ solution containing ~5 M NaCl to maintain an electrolyte concentration similar to that in 15 mM $HAuCl_4$ solution in [BMIM][PF_6]. The products remained a mixture of irregular crystals, similar to the case without 5 M electrolyte, indicating that the electrolyte concentration or ionic strength did not play a key role in the formation of the well-defined, single-crystalline gold dendrites in the IL. However, if the reaction temperature was decreased to room temperature, three-fold symmetrical dendrites with coarse surfaces were obtained after 10 min of reaction in 10 mM aqueous $HAuCl_4$ solution without adding additional electrolytes (Figure 6), which is reminiscent of the nanoparticle-aggregated dendritic gold nanostructures obtained by a similar synthesis procedure.[30] Surprisingly, the XRD pattern shown in Figure 7a exhibited reflections characteristic of a cubic structure AuZn alloy (JCPDS 65-0435), indicating that the dendritic nanostructures obtained in aqueous solution were actually AuZn alloy dendrites rather than metal Au dendrites. The corresponding EDS spectrum (Figure 7b) revealed that the atom ratio of Zn/Au is 49.7:50.2, in good agreement with stoichiometric AuZn within experimental error, confirming the formation of AuZn alloy dendrites in aqueous solution, which is in contrast to the formation of pure gold dendrites in IL solution. It was reported that nanoparticle-aggregated, three-fold symmetrical dendritic gold nanostructures could be obtained by immersing the zinc plate in 1 mM aqueous $HAuCl_4$ solution at room temperature; unfortunately, the related XRD result and composition analysis were not provided to demonstrate the formation of pure gold.[30] In that work, the growth orientation of the dendrite trunk was roughly indexed to be the <211> direction of gold based on the ED result; however, careful examination of the presented ED pattern of a dendrite trunk suggested that the diffraction pattern, which was indexed as the [$\bar{1}$11] zone axis of the gold crystal and used to deduce the <211> growth direction of the trunk, actually did not show a strict six-fold symmetry as assumed, and it could be attributed to the [$12\bar{4}$] zone axis of the AuZn crystal. We have repeated the synthesis by using aqueous $HAuCl_4$ solutions with concentrations ranging from 1 to 10 mM at room temperature and collected the products after different reaction time intervals. XRD measurements were carried out for all the obtained three-fold symmetrical dendrites, which suggested that they were predominantly composed of AuZn crystals. Therefore, we rationally conclude that the reaction between Zn plate and aqueous $HAuCl_4$ solutions actually tended to form AuZn alloy dendrites rather than pure Au dendrites.

It is obvious that the IL [BMIM][PF_6] played an important role in the growth of pure single-crystalline gold dendrites, while the aqueous solution favored the formation of AuZn alloy dendrites made of aggregated primary nanoparticles. As compared to water, ILs show many unique solvent

Table 1. Comparison of Viscosity (η), Conductivity (σ), and Relative Dielectric Constant (ε_r) for Water and [BMIM][PF_6] at 298 K

solvent	η (mPa s)	σ (mS cm^{-1})	ε_r
water	0.8937	4.28[a]	78.54
[BMIM][PF_6]	196−250[b]	1.467[c]	11.4[d]

[a] Conductivity measured for water containing 15 mM $HAuCl_4$. [b] From ref 33. [c] From ref 34. [d] From ref 1.

properties including viscosity, conductivity, solvation capability, and electrochemical properties, which are directly related to the chemical reaction processes in the media. Table 1 summarizes the viscosity (η), conductivity (σ), and relative dielectric constant (ε_r) for the two media water and [BMIM][PF_6]. It can be seen that the viscosity of [BMIM][PF_6] is 2 orders of magnitude larger than that of water, although the reported values varied in a relatively large range (196−250 mPa s), possibly due to the difficulty in experimental measurements and the purity of the IL.[33] Such a high viscosity would significantly slow down the diffusion of reactant ions in the solvent, leading to a much slower rate of diffusion-controlled reactions. The conductivity of [BMIM][PF_6] (1.467 mS cm^{-1}) is somewhat lower than that of water containing 15 mM $HAuCl_4$ (4.28 mS cm^{-1}), and the addition of 15 mM $HAuCl_4$ into [BMIM][PF_6] did not show a noticeable change in the conductivity of the IL. The dielectric constant of [BMIM][PF_6] is considerably lower than that of water, indicating that [BMIM][PF_6] is a less polar solvent.[1a] However, as compared to the effects of viscosity, the effects of conductivity and solvent polarity on the current synthesis reactions could be relatively smaller. Moreover, as described previously, the difference in the ionic strength between the two reaction media did not contribute considerably to reaction processes for Au or AuZn dendrite formation. On the other hand, the redox chemistry in the reaction media could play an important role in the formation of dendritic products on the Zn substrate. It is expected that the potential of the Zn^{2+}/Zn half-cell in an aqueous medium could be very different to that in [BMIM][PF_6]; unfortunately, there are insufficient data on redox potentials for metals for IL systems other than the chloroaluminate-based ILs,[2d] which prevents us from giving a more detailed discussion on the anodic and cathodic half-cell reactions occurring on the surface of Zn in both water and IL. Nevertheless, the reaction processes can be discussed roughly in terms of the driving force for the reaction in the two media. It is known that the diffusivity of reactant ions in IL medium is much smaller than in water[1a] and that the reactivity of the $AuCl_4^-$ ions in IL medium also may be restrained by their interaction with the $[BMIM]^+$ ions. It may be inferred that the driving force for crystallization in the IL solution is considerably lower than that in aqueous solution. As a consequence, single-crystalline symmetrical dendrites were formed in the IL solution due to a smaller driving force, while polycrystalline symmetrical dendrites were formed in the aqueous solution due to a larger driving force.[31] Moreover, the relatively slow reaction rate in ILs could lead to the gradual deposition of pure metal Au, while the reaction rate in aqueous solution was so fast that both Zn^{2+} and $AuCl_4^-$ ions could be reduced at the cathode simultaneously, resulting in the formation of AuZn alloy dendrites rather than pure Au dendrites.

Electrocatalytic Activity of Gold Dendrites. It was reported that gold nanocrystals can exhibit a good electrocatalytic activity for methanol oxidation and that the catalytic property largely depends on their size and shape.[26e,35] Accordingly, the single-crystalline gold dendrites obtained in IL solution were deposited onto the commercial GC electrode to prepare gold dendrite-modified GC electrodes (denoted as gold dendrite electrodes), and their electrocatalytic activity toward the oxidation of methanol was investigated by measuring their cyclic voltammograms in KOH solutions. It was found that the morphology of the gold dendrites on the electrode was retained after continuous potential cycling of more than 40 times. The surface area of the gold dendrite electrode was calculated to be 0.098 cm^2 from the charge consumed during the reduction of surface oxides using the reported value of 400 $\mu C/cm^2$ for a clean Au electrode.[36] This method is a standard electrochemical method frequently used for determining the real surface area of gold, and it has been shown that the value calculated from this method is in close agreement to those obtained by methods using redox probes.[26e] Thereafter, the surface area of all gold electrodes was calculated by this method, and the measured current was normalized with the surface area to obtain the current density. Figure 8a displays the typical CV images recorded of gold dendrite electrodes in 0.1 M KOH solution with and without 2.0 M CH_3OH. In the absence of methanol, the gold dendrite electrode showed a broad oxidation wave at ~0.40 V, which could be ascribed to the formation of gold surface oxides, and a relatively sharp reduction wave at ~0.10 V, which could be attributed to the subsequent removal of the oxides.[21b] When methanol was added, a large anodic wave at 0.254 V was observed for the catalytic oxidation of methanol at the gold dendrite electrode, which may be ascribed to the oxidation of methanol to formates via a four-electron transfer reaction,[34] indicating a considerable electrocatalytic activity for the gold dendrites. During the negative-going potential sweep, the cathodic peak at ~0.1 V corresponding to the reduction of surface oxide was somewhat deceased in the presence of methanol, while a relatively small oxidation current was regained at ~0.1 V, which could be related to the partial removal of the gold surface oxides.[37]

For comparison, the electrocatalytic activity of a commercial polycrystalline Au (abbreviated as poly-Au) electrode, which was first mechanically cleaned and then electrochemically activated with vitriol, also was measured in KOH solution. Figure 8b presents typical CV images of the poly-Au electrode in 0.1 mol dm^{-3} KOH solutions with and without 2.0 M CH_3OH. In the absence of methanol, the

(33) (a) Jin, H.; O'Hare, B.; Dong, J.; Arzhantsev, S.; Baker, G. A.; Wishart, J. F.; Benesi, A. J.; Maronecelli, M. *J. Phys. Chem. B* **2008**, *112*, 81. (b) Pereiro, A. B.; Legido, J. L.; Rodríguez, A. *J. Chem. Thermodyn.* **2007**, *39*, 1168. (c) Jiqin, Z.; Jian, C.; Chengyue, L.; Weiyang, F. *J. Chem. Eng. Data* **2007**, *52*, 812. (d) Zafarani-Moattar, M. T.; Majdan-Cegincara, R. *J. Chem. Eng. Data* **2007**, *52*, 2359. (e) Tokuda, H.; Tsuzuki, S.; Susan, M. A. B. H.; Hayamizu, K.; Watanabe, M. *J. Phys. Chem. B* **2006**, *110*, 19593.

(34) Kanakubo, M.; Harris, K. R.; Tsuchihashi, N.; Ibuki, K.; Ueno, M. *J. Phys. Chem. B* **2007**, *111*, 2062.

(35) (a) Zhong, C. J.; Maye, M. M. *Adv. Mater.* **2001**, *13*, 1507. (b) Maye, M. M.; Luo, J.; Lin, Y. H.; Engelhard, M. H.; Hepel, M.; Zhong, C. J. *Langmuir* **2003**, *19*, 125. (c) Narayanan, R.; El-Sayed, M. A. *J. Phys. Chem. B* **2005**, *109*, 12663. (d) Zhang, J. T.; Liu, P. P.; Ma, H. Y.; Ding, Y. *J. Phys. Chem. C* **2007**, *111*, 10382.

(36) Trasatti, S.; Petrii, O. A. *Pure Appl. Chem.* **1991**, *63*, 711.

(37) Borkowska, Z.; Tymosiak-Zielinska, A.; Shul, G. *Electrochim. Acta* **2004**, *49*, 1209.

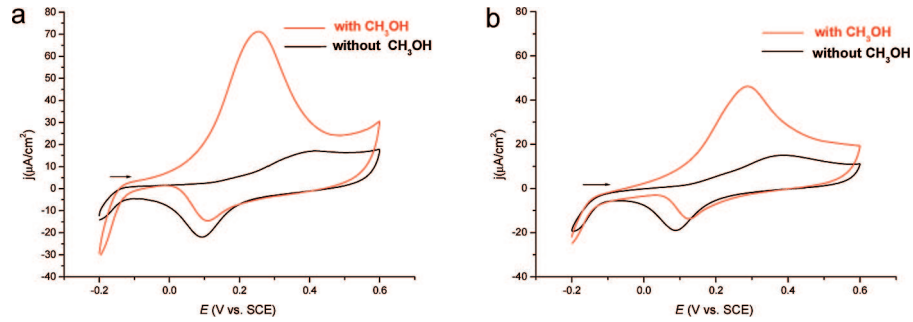

Figure 8. Cyclic voltammograms of gold dendrite electrode (a) and polycrystalline Au electrode (b) in 0.1 mol dm^{-3} KOH solutions without CH_3OH or with 2.0 M CH_3OH. Scan rate was 10 mV s^{-1}.

poly-Au electrode shows a CV curve very similar to that for the gold dendrite electrode (i.e., a broad oxidation wave at ~0.40 V and a relatively sharp reduction wave at ~0.10 V). When methanol was added, however, the poly-Au electrode showed an oxidation peak at 0.287 V, which is 33 mV more positive than the oxidation peak potential for the gold dendrite electrode (0.254 V). Moreover, the current density calculated for methanol oxidation at the poly-Au electrode (26.6 $\mu A/cm^2$) is nearly half of that at the gold dendrite electrode (44.7 $\mu A/cm^2$), indicating that the gold dendrite electrode has a considerably higher electrocatalytic activity toward methanol oxidation than the electrochemically activated poly-Au electrode. In addition, gold nanoparticles with sizes in the range of 50−200 nm were prepared by reducing $HAuCl_4$ in dimethylformamide in the presence of PVP. After a thorough washing, the Au nanoparticles were deposited onto the GC electrode to prepare a gold nanoparticle electrode, which also was used for the measurement of electrocatalytic activity toward the oxidation of methanol under similar conditions. It was revealed that the Au nanoparticle electrode showed an oxidation peak at 0.309 V, which is 55 mV more positive than the oxidation peak potential for the gold dendrite electrode; moreover, the current density for methanol oxidation at the Au nanoparticle electrode was estimated to be 4.1 $\mu A/cm^2$, which is significantly lower than that at both the gold dendrite electrode and the poly-Au electrode. Basically, the high electrocatalytic activity could be related to the hyperbranched morphology of the gold dendrites containing numerous nanorod leaves, which is reminiscent of high electrocatalytic activity toward methanol oxidation observed from the nested gold nanobelt electrode[21b] and the gold nanoflower electrode.[26e] The existence of more defects or hot spots in the gold dendrites could considerably contribute to their higher electrocatalytic activity as compared to both poly-Au and Au nanoparticles. Furthermore, the exposed surfaces with specific crystal planes for the single-crystalline gold dendrites could also contribute to the observed high electrocatalytic activity. Nevertheless, further detailed investigations are needed to elucidate the exact mechanism for the high electrocatalytic activity of single-crystalline gold dendrites.

Conclusion

Hierarchical, three-fold symmetrical, single-crystalline gold nanodendrites successfully were synthesized by simply immersing the zinc plate in a solution of $HAuCl_4$ in the IL [BMIM][PF_6]. It was shown that the unique dendritic gold nanostructures have a three-order hierarchy (i.e., a three-fold symmetrical <111>-oriented trunk, three groups of trident-like <111>-oriented branches grown on the trunk, and many <111>-oriented nanorod leaves grown on the branches symmetrically), indicating an interesting fractal growth. According to the investigation on the growth process of gold dendrites, it was proposed that gold nuclei nanocrystals first formed on the zinc substrate through a direct surface reaction and that the subsequent crystal growth preferentially took place on the preformed gold crystals through a primary cell reaction, leading to the formation of final hyperbranched dendrites under nonequilibrium conditions. The $HAuCl_4$ concentration showed a considerable effect on the growth of the gold dendrites in IL; interestingly, unusual four-branched, <110>-oriented dendrites with a cross-like cross-section were obtained at a lower $HAuCl_4$ concentration. In contrast, AuZn alloy dendrites consisting of aggregated primary nanoparticles were produced when the zinc plate was immersed in an aqueous $AuCl_4$ solution. We propose that the significantly lowered ion diffusivity and reaction rate in the IL medium could largely contribute to the formation of pure single-crystalline gold dendrites. Moreover, electrocatalytic measurements performed in alkaline solution suggest that the obtained dendritic gold nanostructures exhibited a good electrocatalytic activity toward the oxidation of methanol, which might be related to the special three-order hierarchical architectures. These three-fold symmetrical, single-crystalline gold nanodendrites would be ideal candidates for investigating the electrical and photonic properties of hierarchical architectures of 1-D metal nanostructures and could find potential applications in catalysis, biosensing, and nanodevices. This synthetic strategy may open new routes to the ionic liquid-assisted synthesis of inorganic nanostructures with hierarchical architectures as well as functional devices.

Acknowledgment. This work was supported by the NSFC (20673007, 20633010, and 50521201), MOST (2007CB936201), and SRFDP (20070001018).

CM8002386